

# HIGHER TWIST EFFECTS IN PHOTON-PHOTON COLLISIONS

A. I. Ahmadov<sup>1,2,\*</sup>, I. Boztosun<sup>3</sup>, A. Soylyu<sup>3</sup>, and E. A. Dadashov<sup>2</sup>

<sup>1</sup>*Physikalisches Institut, Universität Bonn,  
Nussallee 12, D-53115, Bonn, Germany*

<sup>2</sup>*Institute for Physical Problems, Baku State University,  
Z. Khalilov st. 23, AZ-1148, Baku, Azerbaijan*

<sup>3</sup>*Department of Physics, Faculty of Arts and Sciences,  
Erciyes University, Kayseri, Turkey*

(Dated: July 2, 2018)

## Abstract

In this article, we investigate the contribution of the high twist Feynman diagrams to the large- $p_T$  single pseudoscalar and vector mesons inclusive production cross section in two-photon collisions and we present the general formulae for the high and leading twist differential cross sections. The pion wave function where two non-trivial Gegenbauer coefficients  $a_2$  and  $a_4$  have been extracted from the CLEO data, Braun-Filyanov pion wave function, the asymptotic and the Chernyak-Zhitnitsky wave functions are used in the calculations. For  $\rho$ -meson we used Ball-Braun wave function. The results of all the calculations reveal that the high twist cross sections, the ratio  $R$ , the dependence transverse momentum  $p_T$  and the rapidity  $y$  of meson in the  $\Phi_{CLEO}(x, Q^2)$  wave function case is very close to the  $\Phi_{asy}(x)$  asymptotic wave function case. It is shown that the high twist contribution to the cross section depends on the choice of the meson wave functions.

PACS numbers: 12.38.-t, 13.60.Le, 14.40.Aq, 13.87.Fh,

Keywords: leading twist, high twist, meson wave function

---

\*Electronic address: E-mail:ahmadovazar@yahoo.com

## I. INTRODUCTION

During the last few years, a great deal of progress has been made in the investigation of the properties of hadronic wave functions[1-12]. The notion of distribution amplitudes refers to momentum fraction distributions of partons in meson in particular Fock state with fixed number of compenents. For the minimal number of constituents, the distribution amplitude  $\Phi$  is related to the Bethe-Salpeter wave function  $\Phi_{BS}$  by

$$\Phi(x) \sim \int^{|k_{\perp}| < \mu} d^2 k_{\perp} \Phi_{BS}(x, k_{\perp}). \quad (1.1)$$

The standard approach to distribution amplitudes, which is due to Brodsky and Lepage[13], considers the hadron's parton decomposition in the infinite momentum frame. A conceptually different, but mathematically equivalent formalizm is the light-cone quantiza-tion[14]. Either way, power suppressed contributions to exclusive processes in QCD, which are commonly refered to as higher twist corections. The meson wave functions (also called distribution amplitudes -DA) [1] play a key role in the hard-scattering QCD processes be-cause they encapsulate the essential nonperturbative features of the meson's internal struc-ture in terms of the parton's longitudinal momentum fractions  $x_i$ . Meson wave functions have been extensively studied by using QCD sum rules. The original suggestion by Chernyak and Zhitnitsky of a "double-humped" wave function of the pion at a low scale, far from the asymptotic form, was based on an extraction of the first few moments from a standard QCD sum rule approach[5], which has been criticized and revised in Refs.[6,7]. Subsequently, a number of authors have proposed and studied the modified versions of meson [7,8] and baryon wave functions [9,10]. Additional arguments in favour of a form of the pion wave functions close to the asymptotic one have come from the analysis of the transition form factor  $\gamma\gamma^* \rightarrow \pi^0$  [12]. The measurements of this form factor by the CLEO collaboration are consistent with a near-asymptotic form of the wave function[15]. In [16], the leading-twist wave function of the pion at a low normalization point is calculated in the effective low-energy theory derived from the instanton vacuum. These results for the pion wave function at the low normalization point are close to the asymptotic form and consistent with the CLEO measurements. The authors have obtained a shape substantially different from the Chernyak-Zhitnitsky one because they have chosen a significantly smaller value of the second moment, and, more importantly, they have taken all the moments of the wave function into

account. Their results support the conclusions reached previously in Refs.[6,7]. The QCD factorization theorems predict that the hadron-hadron cross section can be obtained by the convolution of parton distribution functions and a cross section of the corresponding hard scattering subprocess. The parton distributions are nonperturbative, process-independent quantities, which are specific to any given hadron. The hard scattering cross sections are independent of all long distance effects and can be found by means of pQCD. In the framework of pQCD, the higher order corrections to the hard scattering, and therefore to the hadron-hadron process cross sections, have been calculated [17]. These corrections are large and change the leading order results considerably. Other corrections to the hadron-hadron process cross sections and its different characteristics come from the higher twist (HT) terms. By taking these points into account, it may be asserted that the analysis of the higher twist effects on the dependence of the meson wave function in single pseudoscalar and vector meson production at photon-photon collisions are significant in both theoretical and experimental studies. Much effort has recently been devoted to the study of exclusive processes involving large transverse momenta within the context of perturbative quantum chromodynamics (QCD). Here, as in other applications of perturbative QCD, photon-induced reactions play an important role. In [18] have been studied photon-photon annihilation into two mesons at large center-of-mass angles  $\theta_{c.m.}$ . The higher-twist contributions to high- $p_T$  inclusive meson production in two-photon collisions, a single meson inclusive photoproduction and jet photoproduction cross sections were studied by various authors [19-21]. As experiments examining high- $p_T$  particle production in two-photon collisions are improved, it becomes important to reassess the various contributions which arise in quantum chromodynamics. Predictions for the higher-twist contributions, originally obtained in Ref.22, may now be refined using the exclusive-process QCD formalism developed in [23]. Another important aspect of this study is the choice of the meson model wave functions. In this respect, the contribution of the high twist Feynman diagrams to a single meson production cross section in photon-photon collisions has been computed by using various meson wave functions. Also, the leading and high twist contributions have been estimated and compared to each other. Within this context, this paper is organized as follows: in section II, we provide some formulae for the calculation of the contribution of the high twist diagrams. In section III, we provide the formulae for the calculation of the contribution of the leading twist diagrams and in section IV, we present the numerical results for the cross section and discuss the dependence of the

cross section on the meson wave functions. We state our conclusions in section V.

## II. CONTRIBUTION OF THE HIGH TWIST DIAGRAMS

The high twist Feynman diagrams, which describe the subprocess  $\gamma q \rightarrow Mq$  contributes to  $\gamma\gamma \rightarrow MX$  for the meson production in the photon-photon collision are shown in Fig.1(a). The amplitude for this subprocess can be found by means of the Brodsky-Lepage formula [24]

$$M(\hat{s}, \hat{t}) = \int_0^1 dx_1 \int_0^1 dx_2 \delta(1 - x_1 - x_2) \Phi_M(x_1, x_2, Q^2) T_H(\hat{s}, \hat{t}; x_1, x_2). \quad (2.1)$$

In Eq.(2.1),  $T_H$  is the sum of the graphs contributing to the hard-scattering part of the subprocess. The hard-scattering part for the subprocess under consideration is  $\gamma q \rightarrow Mq$ , in which the observed meson is made directly. The hard-scattering amplitude  $T_H(\hat{s}, \hat{t}; x_1, x_2)$  depends on a process and can be obtained in the framework of pQCD, whereas the wave function  $\Phi_M(x_1, x_2, Q^2)$  describes all the non-perturbative and process-independent effects of hadronic binding. The hadron wave function gives the amplitude for finding partons (quarks, gluons) carrying the longitudinal fractional momenta  $\mathbf{x} = (x_1, x_2, \dots, x_n)$  and virtualness up to  $Q^2$  within the hadron and, in general, includes all Fock states with quantum numbers of the hadron. But only the lowest Fock state ( $q_1\bar{q}_2$ -for mesons,  $uud$ -for proton, *etc.*) contributes to the leading scaling behavior, other Fock state contributions are suppressed by powers of  $1/Q^2$ . In our work, we have restricted ourselves to considering the lowest Fock state for a meson. Then  $\mathbf{x} = x_1, x_2$  and  $x_1 + x_2 = 1$ . This approach can be applied not only to the investigation of exclusive processes[25], but also to the calculation of higher twist corrections to some inclusive processes such as large- $p_T$  dilepton production [26], two-jet+meson production in the electron-positron annihilation [27], *ets.* The  $q_1\bar{q}_2$  spin state used in computing  $T_H$  may be written in the form

$$\sum_{s_1, s_2} \frac{u_{s_1}(x_1 p_M) \bar{v}_{s_2}(x_2 p_M)}{\sqrt{x_1} \sqrt{x_2}} \cdot N_{s_1 s_2}^s = \begin{cases} \frac{\gamma_5 \hat{p}_\pi}{\sqrt{2}}, & \pi, \\ \frac{\hat{p}_M}{\sqrt{2}}, & \rho_L \text{ helicity } 0, \\ \mp \frac{\varepsilon_{\pm} \hat{p}_M}{\sqrt{2}}, & \rho_T \text{ helicity } \pm 1, \end{cases} \quad (2.2)$$

where  $\varepsilon_{\pm} = \mp(1/\sqrt{2})(0, 1, \pm i, 0)$  in a frame with  $(p_M)_{1,2} = 0$  and the  $N_{s_1 s_2}^s$  project out a state of spins  $s$ , and  $p_M$  is the four-momentum of the final meson. In our calculation,

we have neglected the meson mass. Turning to extracting the contributions of the high twist subprocesses, there are many kinds of leading twist subprocesses in  $\gamma\gamma$  collisions as the background of the high twist subprocess  $\gamma q \rightarrow Mq$ , such as  $\gamma + \gamma \rightarrow q + \bar{q}$ . The contributions from these leading twist subprocesses strongly depend on some phenomenological factors, for example, quark and gluon distribution functions in meson and fragmentation functions of various constituents *etc.* Most of these factors have not been well determined, neither theoretically nor experimentally. Thus they cause very large uncertainty in the computation of the cross section of process  $\gamma\gamma \rightarrow MX$ . In general, the magnitude of this uncertainty is much larger than the sum of all the high twist contributions, so it is very difficult to extract the high twist contributions.

The Mandelstam invariant variables for subprocesses  $\gamma q \rightarrow Mq$  are defined as

$$\hat{s} = (p_1 + p_\gamma)^2, \quad \hat{t} = (p_\gamma - p_M)^2, \quad \hat{u} = (p_1 - p_M)^2. \quad (2.3)$$

In our calculation, we have also neglected the quark masses. We have aimed to calculate the single meson production cross section and to fix the differences due to the use of various meson wave functions. We have used six different functions: the asymptotic wave function ASY, the Chernyak-Zhitnitsky [2,5] and the wave function in which two non-trivial Gegenbauer coefficients  $a_2$  and  $a_4$  have been extracted from the CLEO data on the  $\gamma\gamma^* \rightarrow \pi^0$  transition form factor [28] and Braun-Filyanov wave function [7]. In ref.[28], the authors have used the QCD light-cone sum rules approach and have included into their analysis the NLO perturbative and twist-four corrections. They found that in the model with two nonasymptotic terms, at the scale  $\mu_0 = 2.4\text{GeV}$ . For  $\rho$ -meson we used Ball-Braun wave function [29]. In order to proceed to numerical calculations we have to use the explicit expressions for the  $\rho$  meson wave functions. They are defined by means of the following formulas: For the longitudinally polarized  $\rho$  meson,  $\rho_L \equiv \rho_{h=0}$

$$\langle 0 | \bar{d}(z)\gamma_\mu u(-z) | \rho_L(p) \rangle = f_\rho^L p_\mu \int_{-1}^1 d\xi e^{i\xi(zP)} \phi_L^\rho(\xi), \quad (2.4)$$

for the transversely polarized  $\rho$  meson,  $\rho_T \equiv \rho_{h=\pm 1}$

$$\langle 0 | \bar{d}(z)\sigma_{\mu\nu} I u(-z) | \rho_T(p) \rangle = f_\rho^T (\epsilon_\mu^T p_\nu - \epsilon_\nu^T p_\mu) \int_{-1}^1 d\xi e^{i\xi(zP)} \phi_T^\rho(\xi), \quad (2.5)$$

$f_\rho^L, f_\rho^T$  are the dimensional constants which determine the values of the wave functions at the origin, and

$$I = \exp \left[ ig \int_{-z}^z d\sigma_\mu A^\mu(\sigma) \right] \quad (2.6)$$

In Eqs.(2.4), (2.5) and (2.6),  $\bar{d}(z)$ ,  $u(z)$  and  $A_\mu(\sigma)$  are quark and gluon fields,  $\epsilon_\mu^T$  is the polarization vector, and  $|\rho_L(p)\rangle$ ,  $|\rho_T(p)\rangle$  are the longitudinally and transversely polarized  $\rho$  meson states with the momentum  $p$ .

$$\Phi_{asy}(x) = \sqrt{3}f_\pi x(1-x), \quad \Phi_{L(T)}^{asy}(x) = \sqrt{6}f_\rho^{L(T)}x(1-x)$$

$$\Phi_{CZ}(x, \mu_0^2) = 5\Phi_{asy}(2x-1)^2, \quad \Phi_{L(T)}^\rho(x, \mu_0^2) = \Phi_{L(T)}^{asy}(x) [a + b(2x-1)^2],$$

$$\Phi_{BF}(x, \mu_0^2) = \Phi_{asy}(x)[1 + 0.66(5(2x-1)^2 - 1) + 0.4687(21(2x-1)^4 - 14(2x-1)^2 + 1)],$$

$$\Phi_{CLEO}(x, \mu_0^2) = \Phi_{asy}(x)[1 + 0.285(5(2x-1)^2 - 1) - 0.263(21(2x-1)^4 - 14(2x-1)^2 + 1)], \quad (2.7)$$

where  $f_\pi=0.0923$  GeV,  $f_\rho^L=0.141$  GeV,  $f_\rho^T=0.16$  GeV is the pion and  $\rho$  mesons decay constants,  $a = 0.7$ ,  $b = 1.5$  for both longitudinally and transversely polarized  $\rho$  meson[29]. Here, we have denoted by  $x \equiv x_1$ , the longitudinal fractional momentum carried by the quark within the meson. Then,  $x_2 = 1 - x$  and  $x_1 - x_2 = 2x - 1$ . The pion and  $\rho$  meson wave function is symmetric under replacement  $x_1 - x_2 \leftrightarrow x_2 - x_1$ . The values of the pion wave function moments  $\langle \xi^n \rangle$  are defined as

$$\langle \xi^n \rangle = \int_{-1}^1 d\xi \xi^n \tilde{\Phi}_\pi(\xi) \quad (2.8)$$

Here,  $\tilde{\Phi}_\pi(\xi)$  is the model function without  $f_\pi$  and  $\xi = x_1 - x_2$ . The pion wave function moments have been calculated by means of the QCD sum rules method by Chernyak and Zhitnitsky at the normalization point  $\mu_0 = 0.5\text{GeV}$ . They are equal to

$$\langle \xi^0 \rangle_{\mu_0} = 1, \quad \langle \xi^2 \rangle_{\mu_0} = 0.44, \quad \langle \xi^4 \rangle_{\mu_0} = 0.27 \quad (2.9)$$

The Chernyak-Zhitnitsky pion model wave function has the following moments

$$\langle \xi^0 \rangle_{\mu_0} = 1, \quad \langle \xi^2 \rangle_{\mu_0} = 0.43, \quad \langle \xi^4 \rangle_{\mu_0} = 0.24 \quad (2.10)$$

It is interesting to note that the corresponding moments of the asymptotic wave function differ considerably from those in Eqs.(2.9), (2.10)

$$\langle \xi^0 \rangle_{\mu_0} = 1, \quad \langle \xi^2 \rangle_{\mu_0} = 0.20, \quad \langle \xi^4 \rangle_{\mu_0} = 0.086 \quad (2.11)$$

This means that the realistic pion wave function is much wider than the asymptotic one [5,30]. The model functions can be written as

$$\Phi_{asy}(x) = \sqrt{3}f_\pi x(1-x),$$

$$\begin{aligned}
\Phi_{CZ}(x, \mu_0^2) &= \Phi_{asy}(x) \left[ C_0^{3/2}(2x-1) + \frac{2}{3}C_2^{3/2}(2x-1) \right], \\
\Phi_{L(T)}^\rho(x, \mu_0^2) &= \Phi_{L(T)}^{asy}(x) \left[ C_0^{3/2}(2x-1) + 0.18(0.2)\frac{2}{3}C_2^{3/2}(2x-1) \right], \\
\Phi_{BF}(x, \mu_0^2) &= \Phi_{asy}(x) \left[ C_0^{3/2}(2x-1) + 0.44C_2^{3/2}(2x-1) + 0.25C_4^{3/2}(2x-1) \right] \\
\Phi_{CLEO}(x, \mu_0^2) &= \Phi_{asy}(x) \left[ C_0^{3/2}(2x-1) + 0.19C_2^{3/2}(2x-1) - 0.14C_4^{3/2}(2x-1) \right], \\
C_0^{3/2}(2x-1) &= 1, \quad C_2^{3/2}(2x-1) = \frac{3}{2}(5(2x-1)^2 - 1), \\
C_4^{3/2}(2x-1) &= \frac{15}{8}(21(2x-1)^4 - 14(2x-1)^2 + 1). \tag{2.12}
\end{aligned}$$

It may be seen that the pion wave function extracted from the experimental data depends on the methods used and their accuracy. Although one may claim that the meson wave function is a process-independent quantity, describing the internal structure of the meson itself, the exploration of different exclusive processes with the same meson leads to a variety of wave functions. This means that the methods employed have shortcomings or do not encompass all the mechanisms important for a given process. Such a situation is pronounced in the case of the pion. It is known that the meson wave function (distribution amplitude-DA) can be expanded over the eigenfunctions of the one-loop Brodsky-Lepage equation, *i.e.*, in terms of the Gegenbauer polynomials  $\{C_n^{3/2}(2x-1)\}$ ,

$$\Phi_M(x, Q^2) = \Phi_{asy}(x) \left[ 1 + \sum_{n=2,4,\dots}^{\infty} a_n(Q^2) C_n^{3/2}(2x-1) \right], \tag{2.13}$$

The evolution of the wave function (DA) on the factorization scale  $Q^2$  is governed by the functions  $a_n(Q^2)$ ,

$$\begin{aligned}
a_n(Q^2) &= a_n(\mu_0^2) \left[ \frac{\alpha_s(Q^2)}{\alpha_s(\mu_0^2)} \right]^{\gamma_n/\beta_0}, \\
\frac{\gamma_2}{\beta_0} &= \frac{50}{81}, \quad \frac{\gamma_4}{\beta_0} = \frac{364}{405}, \quad n_f = 3.
\end{aligned} \tag{2.14}$$

In Eq.(2.14),  $\{\gamma_n\}$  are anomalous dimensions defined by the expression,

$$\gamma_n = C_F \left[ 1 - \frac{2}{(n+1)(n+2)} + 4 \sum_{j=2}^{n+1} \frac{1}{j} \right]. \tag{2.15}$$

The constants  $a_n(\mu_0^2) = a_n^0$  are input parameters that form the shape of the wave functions and which can be extracted from experimental data or obtained from the nonperturbative

QCD computations at the normalization point  $\mu_0^2$ . The QCD coupling constant  $\alpha_s(Q^2)$  at the two-loop approximation is given by the expression

$$\alpha_s(Q^2) = \frac{4\pi}{\beta_0 \ln(Q^2/\Lambda^2)} \left[ 1 - \frac{2\beta_1}{\beta_0^2} \frac{\ln \ln(Q^2/\Lambda^2)}{\ln(Q^2/\Lambda^2)} \right]. \quad (2.16)$$

Here,  $\Lambda$  is the QCD scale parameter,  $\beta_0$  and  $\beta_1$  are the QCD beta function one- and two-loop coefficients, respectively,

$$\beta_0 = 11 - \frac{2}{3}n_f, \quad \beta_1 = 51 - \frac{19}{3}n_f.$$

For completeness we give the sum rules for the  $\rho$ -meson wave functions moments  $\langle \xi \rangle = \int d\xi \xi^n \phi(u, \mu)$  [29].

$$(f_\rho^\perp)^2(\mu) \langle \xi^n \rangle_\perp e^{-m_\rho^2/M^2} = \frac{3}{2\pi^2} \int_0^{s_0} ds \int_0^1 du e^{-s/M^2} u \bar{u} (2u-1)^n.$$

$$\left\{ 1 + \frac{\alpha_s}{3\pi} \left( 6 - \frac{\pi^2}{3} + 2 \ln \frac{s}{\mu^2} + \ln u + \ln \bar{u} + \ln^2 \frac{u}{\bar{u}} \right) \right\} + \frac{n-1}{n+1} \frac{1}{12M^2} \langle \frac{\alpha_s}{\pi} G^2 \rangle +$$

$$\frac{64\pi}{81M^4} (n-1) \langle \sqrt{\alpha_s} \bar{q} q \rangle^2, \quad (2.17)$$

$$f_\rho^2 \langle \xi \rangle_\parallel e^{-m_{\rho^2}/M^2} = \frac{3}{4\pi^2(n+1)(n+3)} \left( 1 + \frac{\alpha_s}{\pi} A'_n \right) M^2 (1 - e^{-s_0/M^2}) +$$

$$\frac{1}{12M^2} \langle \frac{\alpha_s}{\pi} G^2 \rangle + \frac{16\pi}{81M^4} (4n-7) \langle \sqrt{\alpha_s} \bar{q} q \rangle^2. \quad (2.18)$$

Here the vacuum condensates are equal to [31]

$$\langle \frac{\alpha_s}{\pi} G^2 \rangle = (0.012 \pm 0.006) GeV^4$$

$$\langle \sqrt{\alpha_s} \bar{q} q \rangle^2 = 0.56 (-0.25 GeV)^6$$

The higher-twist subprocess  $\gamma q \rightarrow Mq$  contributes to  $\gamma\gamma \rightarrow MX$  through the diagram of Fig.1(a). We now incorporate the higher-twist(HT) subprocess  $\gamma q \rightarrow Mq$  into the full inclusive cross section. In this subprocess  $\gamma q \rightarrow Mq$ , photon and the meson may be viewed as an effective current striking the incoming quark line. With this in mind, we write the complete cross section in formal analogy with deep-inelastic scattering,

$$E \frac{d\sigma}{d^3p}(\gamma\gamma \rightarrow MX) = \frac{3}{\pi} \sum_{q\bar{q}} \int_0^1 dx \delta(\hat{s} + \hat{t} + \hat{u}) \hat{s} G_{q/\gamma}(x, -\hat{t}) \frac{d\sigma}{dt}(\gamma q \rightarrow Mq) + (t \leftrightarrow u), \quad (2.19)$$



Here  $G_{q/\gamma}$  is the per color distribution function for a quark in a photon. The subprocess cross section for  $\pi, \rho_L$  and  $\rho_T$  production

$$\frac{d\sigma}{dt}(\gamma q \rightarrow Mq) = \begin{cases} \frac{8\pi\alpha_E C_F}{9} [D(\hat{s}, \hat{u})]^2 \frac{1}{\hat{s}^2(-\hat{t})} \left[ \frac{1}{\hat{s}^2} + \frac{1}{\hat{u}^2} \right], & M = \pi, \rho_L, \\ \frac{8\pi\alpha_E C_F}{9} [D(\hat{s}, \hat{u})]^2 \frac{8(-\hat{t})}{\hat{s}^4 \hat{u}^2}, & M = \rho_T, \end{cases} \quad (2.20)$$

where

$$D(\hat{s}, \hat{u}) = \hat{u} e_1 \alpha_s \left( \frac{\hat{s}}{2} \right) I_M \left( \frac{\hat{s}}{2} \right) + \hat{s} e_2 \alpha_s \left( \frac{-\hat{u}}{2} \right) I_M \left( \frac{-\hat{u}}{2} \right)$$

where  $Q_1^2 = \hat{s}/2$ ,  $Q_2^2 = -\hat{u}/2$ , represents the momentum squared carried by the hard gluon in Fig.1(a),  $e_1(e_2)$  is the charge of  $q_1(\bar{q}_2)$  and  $C_F = \frac{4}{3}$ .

The  $I_M$  factors reflect the exclusive form factor of the meson and are discussed thoroughly in [20], as is the motivation the arguments of  $\alpha_s$  and  $I_M$ . Note that the relation between  $I_M$  and the meson form factor completely fixes the normalization of the higher-twist subprocess. The full cross section for  $\pi$  and  $\rho_L$  production is given by

$$E \frac{d\sigma}{d^3p}(\gamma\gamma \rightarrow MX) = \frac{s}{s+u} \sum_{q\bar{q}} G_{q/\gamma}(x, -\hat{t}) \frac{8\pi\alpha_E C_F}{3} \frac{[D(\hat{s}, \hat{u})]^2}{\hat{s}^2(-\hat{t})} \left[ \frac{1}{\hat{s}^2} + \frac{1}{\hat{u}^2} \right] + \frac{s}{s+t} \sum_{q\bar{q}} G_{q/\gamma}(x, -\hat{u}) \frac{8\pi\alpha_E C_F}{3} \frac{[D(\hat{s}, \hat{t})]^2}{\hat{s}^2(-\hat{u})} \left[ \frac{1}{\hat{s}^2} + \frac{1}{\hat{t}^2} \right], \quad (2.21)$$

In (2.21), the subprocess invariants are

$$\begin{aligned} \hat{s} &= xs, \\ \hat{t} &= t, \\ \hat{u} &= xu, \end{aligned} \quad (2.22)$$

$$\begin{aligned} t &= -\frac{s}{2}(x_R - x_F) = -m_T \sqrt{s} e^{-y}, \\ u &= -\frac{s}{2}(x_R + x_F) = -m_T \sqrt{s} e^y, \end{aligned}$$

with  $x_R = (x_F^2 + x_T^2)^{1/2}$ . Here  $x_F = 2(p_M)_\parallel / \sqrt{s}$  and  $x_T = 2(p_M)_\perp / \sqrt{s} = 2p_T / \sqrt{s}$  specify the longitudinal and transverse momentum of the meson. In terms of these the rapidity of  $M$  is given by

$$y = \frac{1}{2}[(x_R + x_F)/(x_R - x_F)]$$

where  $m_T$  – is the transverse mass of meson, which is given by

$$m_T = \sqrt{m^2 + p_T^2}$$

As seen from (2.20) the subprocess cross section for longitudinal  $\rho_L$  production is very similar to that for  $\pi$  production, but the transverse  $\rho_T$  subprocess cross section has a quite different form. We have extracted the following high twist subprocesses contributing to the two covariant cross sections in Eq.(2.19)

$$\gamma q_1 \rightarrow (q_1 \bar{q}_2) q_1 \quad , \quad \gamma \bar{q}_2 \rightarrow (q_1 \bar{q}_2) \bar{q}_2 \quad (2.23)$$

As seen from Eq.(2.21), at fixed  $p_T$ , the cross section falls very slowly with  $s$ . Also, at fixed  $s$ , the cross section decreases as  $1/p_T^5$ , multiplied by a slowly varying logarithmic function which vanishes at the phase-space boundary. Thus, the  $p_T$  spectrum is fairly independent of  $s$  except near the kinematic limit.

### III. CONTRIBUTION OF THE LEADING TWIST DIAGRAMS

Regarding the high twist corrections to the meson production cross section, a comparison of our results with leading twist contributions is crucial. The contribution from the leading-twist subprocess  $\gamma\gamma \rightarrow q\bar{q}$  is shown in Fig.1(b). The corresponding inclusive cross section for production of a meson  $M$  is given by

$$\left[ \frac{d\sigma}{d^3p} \right]_{\gamma\gamma \rightarrow MX} = \frac{3}{\pi} \sum_{q,\bar{q}} \int_0^1 \frac{dz}{z^2} \delta(\hat{s} + \hat{t} + \hat{u}) \hat{s} D_q^M(z, -\hat{t}) \frac{d\sigma}{d\hat{t}}(\gamma\gamma \rightarrow q\bar{q}) \quad (3.1)$$

where

$$\hat{s} = s, \quad \hat{t} = \frac{t}{z}, \quad \hat{u} = \frac{u}{z}$$

Here  $s$ ,  $t$ , and  $u$  refer to the overall  $\gamma\gamma \rightarrow MX$  reaction.  $D_q^M(z, -\hat{t})$  represents the quark fragmentation function into a meson containing a quark of the same flavor. For  $\pi^+$  production we assume  $D_{\pi^+/u} = D_{\pi^+/\bar{d}}$ . In the leading twist subprocess, meson is indirectly emitted from the quark with fractional momentum  $z$ . The  $\delta$  function may be expressed in terms of the parton kinematic variables, and the  $z$  integration may then be done. The final form for the leading-twist contribution to the large- $p_T$  meson production cross section in the process  $\gamma\gamma \rightarrow MX$  is

$$\begin{aligned} \Sigma_M^{LT} \equiv E \frac{d\sigma}{d^3P} &= \frac{3}{\pi} \sum_{q,\bar{q}} \int_0^1 \frac{dz}{z^2} \delta(\hat{s} + \hat{t} + \hat{u}) \hat{s} D_q^M(z, -\hat{t}) \frac{d\sigma}{d\hat{t}}(\gamma\gamma \rightarrow q\bar{q}) = \\ &= \frac{3}{\pi} \sum_{q,\bar{q}} \int_0^1 d\frac{1}{z} \delta(s + \frac{1}{z}(t + u)) \hat{s} D_q^M(z, -\hat{t}) \frac{d\sigma}{d\hat{t}}(\gamma\gamma \rightarrow q\bar{q}) = \frac{34}{27} \alpha_E^2 \frac{1}{z} D_q^M(z) \frac{1}{\hat{s}^2} \left[ \frac{\hat{t}}{\hat{u}} + \frac{\hat{u}}{\hat{t}} \right] \end{aligned} \quad (3.2)$$

where

$$z = -\frac{t+u}{s}$$

We should note that  $D(z, -\hat{t})/z$  behaves as  $1/z^2$  as  $z \rightarrow 0$ . For the kinematic range considered in our numerical calculations,  $D(z, -\hat{t})/z$  increases even more rapidly. We obtain of the final cross section, Eq.(3.2), are as follows: At fixed  $p_T$ , the cross section decreases with  $s$  asymptotically as  $1/s$ . At fixed  $s$ , the  $D(z, -\hat{t})$  function causes the cross section to decrease rapidly as  $p_T$  increases towards the phase-space boundary ( $z \rightarrow 1$ ). As  $s$  increases, the phase-space boundary moves to higher  $p_T$ , and the  $p_T$  distribution broadens.

#### IV. NUMERICAL RESULTS AND DISCUSSION

In this section, the numerical results for higher twist effects on the dependence of the chosen meson wave functions in the process  $\gamma\gamma \rightarrow MX$  are discussed. We have calculated the dependence on the meson wave functions for the high twist contribution to the large- $p_T$  single pseudoscalar  $\pi^+$  and vector  $\rho_L^+$ ,  $\rho_T^+$  mesons production cross section in the photon-photon collision. The  $\pi^-$ ,  $\rho_L^-$ ,  $\rho_T^-$  cross sections are, of course, identical. In the calculations, the asymptotic  $\Phi_{asy}$ , Chernyak-Zhitnitsky  $\Phi_{CZ}$ , Braun-Filyanov wave function[7], and also, the pion wave function, from which two non-trivial Gegenbauer coefficients  $a_2$  and  $a_4$  have been extracted from the CLEO data on the  $\pi^0\gamma$  transition form factor have been used[20]. For  $\rho$ -meson we used Ball-Braun wave function[29]. In the ref.[28], authors have used the QCD light-cone sum rules approach and included into their analysis the NLO perturbative and twist-four corrections. For the high twist subprocess, we take  $\gamma q \rightarrow Mq$  and we have extracted the following two high twist subprocess  $\gamma q_1 \rightarrow (q_1\bar{q}_2)q_1$ ,  $\gamma\bar{q}_2 \rightarrow (q_1\bar{q}_2)\bar{q}_2$  contributing to  $\gamma\gamma \rightarrow MX$  cross sections. Inclusive meson photoproduction represents a significant test case in which higher-twist terms dominate those of leading twist in certain kinematic domains. For the dominant leading twist subprocess for the meson production, we take the photon-photon annihilation  $\gamma\gamma \rightarrow q\bar{q}$ , in which the  $M$  meson is indirectly emitted from the quark. As an example for the quark distribution function inside the photon has been used [32]. The quark fragmentation function has been taken from [33]. The other problems dealt with are the choice of the QCD scale parameter  $\Lambda$  and the number of the active quark flavors  $n_f$ . The high twist subprocesses probe the meson wave functions over a large range of  $Q^2$  squared momentum transfer, carried by the gluon. Therefore, we take

$Q_1^2 = \hat{s}/2$ ,  $Q_2^2 = -\hat{u}/2$  which we have obtained directly from the high twist subprocesses diagrams. The same  $Q^2$  has been used as an argument of  $\alpha_s(Q^2)$  in the calculation of each diagram. The results of our numerical calculations are plotted in Figs.2-7. Figs.2-3 show the dependence of the differential cross sections of the high twist  $\Sigma_M^{HT}$ , and ratio  $R = \Sigma_M^{HT}/\Sigma_M^{LT}$  as a function of the meson transverse momentum  $p_T$  for six different meson wave functions. As shown in Fig.2, the high twist differential cross section is monotonically decreasing with an increase in the transverse momentum of the meson. As seen from Fig.2, in all wave functions of the mesons, the dependencies of the high twist cross sections on the  $p_T$  transverse momentum of the meson demonstrate the same behavior. Also, as seen from Fig.2 the leading twist cross section is 2-4 order suppress the high twist cross section in magnitude, on the dependence wave functions of meson, respectively. On the other hand, the higher twist corrections are very sensitive to the choice of the meson wave function. We should note that the magnitude of the high twist cross section in the pion wave function  $\Phi_{CLEO}(x, Q^2)$  case is very close to the asymptotic wave function  $\Phi_{asy}(x)$  case. In Fig.3, the ratio  $R = \Sigma_M^{HT}/\Sigma_M^{LT}$  is plotted at  $y = 0$  as a function of the meson transverse momentum  $p_T$  for the different meson wave functions. First of all, it is seen that the values of  $R$  for fixed  $y$  and  $\sqrt{s}$  depend on the choice of the meson wave function. Also, the distinction between  $R(\Phi_{asy}(x))$  with  $R(\Phi_{CLEO}(x, Q^2))$ ,  $R(\Phi_{CZ}(x, Q^2))$ ,  $R(\Phi_{BF}(x, Q^2))$ ,  $R(\Phi_{\rho_L}(x, Q^2))$  and  $R(\Phi_{\rho_T}(x, Q^2))$  have been calculated. We have found that the distinction  $R(\Phi_{asy}(x))$  and  $R(\Phi_{CLEO}(x, Q^2))$  is small, whereas a distinction between  $R(\Phi_{asy}(x))$  with  $R(\Phi_{CZ}(x, Q^2))$ ,  $R(\Phi_{BF}(x, Q^2))$ ,  $R(\Phi_{\rho_L}(x, Q^2))$  and  $R(\Phi_{\rho_T}(x, Q^2))$  is significant. For example, in the case of  $\sqrt{s} = 89\text{GeV}$ ,  $y = 0$ , the distinction between  $R(\Phi_{asy}(x))$  with  $R(\Phi_i(x, Q^2))$  ( $i = CLEO, CZ, BF, BB(L), BB(T)$ ) is shown in Table I. Thus, the distinction between  $R(\Phi_{asy}(x))$  and  $R(\Phi_{CLEO}(x, Q^2))$  is maximum at  $p_T = 14\text{GeV}/c$ , but the distinction between  $R(\Phi_{asy}(x))$  with  $R(\Phi_{CZ}(x, Q^2))$ ,  $R(\Phi_{BF}(x, Q^2))$ ,  $R(\Phi_{\rho_L}(x, Q^2))$  and  $R(\Phi_{\rho_T}(x, Q^2))$  is maximum at  $p_T = 2\text{GeV}/c$  and decreases with an increase in  $p_T$ . Such a behavior of  $R$  may be explained by reducing all moments of the meson model wave functions to those of  $\Phi_{asy}(x)$  for high  $Q^2$ . In Fig.4, the ratio  $R = \Sigma_M^{HT}/\Sigma_M^{LT}$  is plotted at  $p_T = 7\text{GeV}/c$  as a function of the rapidity  $y$  of the meson for the different meson wave functions. As we are now in the high energy region, the change of the rapidity to determine these relations is given by  $-\ln(\sqrt{s}/p_T) \leq y \leq \ln(\sqrt{s}/p_T)$ . At  $\sqrt{s} = 89\text{GeV}$  and  $p_T = 7\text{GeV}/c$ , the meson rapidity lies in the region  $-2.543 \leq y \leq 2.543$ . First of all, it is seen that the values of  $R$  for fixed  $p_T$  and

$\sqrt{s}$  depend on the choice of the meson wave function. As shown in Fig.4 in all wave functions of the mesons, the dependencies of the ratio  $R = \Sigma_M^{HT}/\Sigma_M^{LT}$  of the rapidity  $y$  of the meson has a minimum approximately at one point  $y = 1.75$ . After this point, the ratio increases with increasing  $y$ . Also, the distinction between  $R(\Phi_{asy}(x))$  with  $R(\Phi_{CLEO}(x, Q^2))$ ,  $R(\Phi_{CZ}(x, Q^2))$ ,  $R(\Phi_{BF}(x, Q^2))$ ,  $R(\Phi_{\rho_L}(x, Q^2))$  and  $R(\Phi_{\rho_T}(x, Q^2))$  have been calculated. We have found that the distinction  $R(\Phi_{asy}(x))$  and  $R(\Phi_{CLEO}(x, Q^2))$  is small, whereas a distinction between  $R(\Phi_{asy}(x))$  with  $R(\Phi_{CZ}(x, Q^2))$ ,  $R(\Phi_{BF}(x, Q^2))$ ,  $R(\Phi_{\rho_L}(x, Q^2))$  and  $R(\Phi_{\rho_T}(x, Q^2))$  is significant. For example, in the case of  $\sqrt{s} = 89\text{GeV}$ ,  $p_T = 7\text{GeV}/c$ , the distinction between  $R(\Phi_{asy}(x))$  with  $R(\Phi_i(x, Q^2))$  ( $i = CLEO, CZ, BF, BB(L), BB(T)$ ) is presented in Table II. Thus, the distinction between  $R(\Phi_{asy}(x))$  and  $R(\Phi_{CLEO}(x, Q^2))$  is maximum at  $y = -2.25$ , but the distinction between  $R(\Phi_{asy}(x))$  with  $R(\Phi_{CZ}(x, Q^2))$ ,  $R(\Phi_{BF}(x, Q^2))$ ,  $R(\Phi_{\rho_L}(x, Q^2))$  and  $R(\Phi_{\rho_T}(x, Q^2))$  is maximum at  $y = 1.75$  and decreases with an increase in  $y$ . Such a behavior of  $R$  may be explained by reducing all moments of the pion model wave functions to those of  $\Phi_{asy}(x)$  for high  $Q^2$ . We have also carried out comparative calculations in the center-of-mass energy  $\sqrt{s} = 209\text{GeV}$ . Figs.5-6 show the dependence of the differential cross sections of the high twist  $\Sigma_M^{HT}$ , and ratio  $R = \Sigma_M^{HT}/\Sigma_M^{LT}$  as a function of the meson transverse momentum  $p_T$  for six different meson wave functions. As shown in Fig.5, the high twist differential cross section is monotonically decreasing with an increase in the transverse momentum of the meson. As seen from Fig.5, in all wave functions of the mesons, the dependencies of the high twist cross sections on the  $p_T$  transverse momentum of the meson demonstrate the same behavior. Also, as seen from Fig.5 the leading twist cross section is 4-5 order suppress the high twist cross section in magnitude, on the dependence wave functions of meson, respectively. Also here, as in Fig.2 the higher twist corrections are very sensitive to the choice of the meson wave function. We should note that the magnitude of the high twist cross section in the pion wave function  $\Phi_{CLEO}(x, Q^2)$  case is very close to the asymptotic wave function  $\Phi_{asy}(x)$  case. In Fig.6, the ratio  $R = \Sigma_M^{HT}/\Sigma_M^{LT}$  is plotted at  $y = 0$  as a function of the meson transverse momentum  $p_T$  for the different meson wave functions. First of all, it is seen that the values of  $R$  for fixed  $y$  and  $\sqrt{s}$  depend on the choice of the meson wave function. Also, the distinction between  $R(\Phi_{asy}(x))$  with  $R(\Phi_{CLEO}(x, Q^2))$ ,  $R(\Phi_{CZ}(x, Q^2))$ ,  $R(\Phi_{BF}(x, Q^2))$ ,  $R(\Phi_{\rho_L}(x, Q^2))$  and  $R(\Phi_{\rho_T}(x, Q^2))$  have been calculated. We have found that the distinction  $R(\Phi_{asy}(x))$  and  $R(\Phi_{CLEO}(x, Q^2))$  is small, whereas a distinction between  $R(\Phi_{asy}(x))$  with  $R(\Phi_{CZ}(x, Q^2))$ ,  $R(\Phi_{BF}(x, Q^2))$ ,  $R(\Phi_{\rho_L}(x, Q^2))$  and  $R(\Phi_{\rho_T}(x, Q^2))$  is signif-

icant. For example, in the case of  $\sqrt{s} = 209\text{GeV}$ ,  $y = 0$ , the distinction between  $R(\Phi_{asy}(x))$  with  $R(\Phi_i(x, Q^2))$  ( $i = CLEO, CZ, BF, BB(L), BB(T)$ ) is shown in Table III. Thus, the distinction between  $R(\Phi_{asy}(x))$  with  $R(\Phi_{CLEO}(x, Q^2))$ ,  $R(\Phi_{CZ}(x, Q^2))$  and  $R(\Phi_{BF}(x, Q^2))$  is maximum at  $p_T = 20\text{GeV}/c$ , but the distinction between  $R(\Phi_{asy(LT)}(x))$  with  $R(\Phi_{\rho_L}(x, Q^2))$  and  $R(\Phi_{\rho_T}(x, Q^2))$  is maximum at  $p_T = 100\text{GeV}/c$  and decreases with an increase in  $p_T$ . In Fig.7, the ratio  $R = \Sigma_M^{HT}/\Sigma_M^{LT}$  is plotted at  $p_T = 17\text{GeV}/c$  as a function of the rapidity  $y$  of the meson for the different meson wave functions. At  $\sqrt{s} = 209\text{GeV}$  and  $p_T = 17\text{GeV}/c$ , the meson rapidity lies in the region  $-2.509 \leq y \leq 2.509$ . First of all, it is seen that the values of  $R$  for fixed  $p_T$  and  $\sqrt{s}$  depend on the choice of the meson wave function. Also, the distinction between  $R(\Phi_{asy}(x))$  with  $R(\Phi_{CLEO}(x, Q^2))$ ,  $R(\Phi_{CZ}(x, Q^2))$ ,  $R(\Phi_{BF}(x, Q^2))$ ,  $R(\Phi_{\rho_L}(x, Q^2))$  and  $R(\Phi_{\rho_T}(x, Q^2))$  have been calculated. We have found that the distinction  $R(\Phi_{asy}(x))$  and  $R(\Phi_{CLEO}(x, Q^2))$  is small, whereas a distinction between  $R(\Phi_{asy}(x))$  with  $R(\Phi_{CZ}(x, Q^2))$ ,  $R(\Phi_{BF}(x, Q^2))$ ,  $R(\Phi_{\rho_L}(x, Q^2))$  and  $R(\Phi_{\rho_T}(x, Q^2))$  is significant. For example, in the case of  $\sqrt{s} = 209\text{GeV}$ ,  $p_T = 17\text{GeV}/c$ , the distinction between  $R(\Phi_{asy}(x))$  with  $R(\Phi_i(x, Q^2))$  ( $i = CLEO, CZ, BF, BB(L), BB(T)$ ) is shown in Table IV. Thus, the distinction between  $R(\Phi_{asy}(x))$  and  $R(\Phi_{CLEO}(x, Q^2))$  is maximum at  $y = -2.25$ , but the distinction between  $R(\Phi_{asy}(x))$  with  $R(\Phi_{CZ}(x, Q^2))$ ,  $R(\Phi_{BF}(x, Q^2))$ ,  $R(\Phi_{\rho_L}(x, Q^2))$  and  $R(\Phi_{\rho_T}(x, Q^2))$  is maximum at  $y = 1.75$  and decreases with an increase in  $y$ . Also, as seen from Fig.7 in all wave functions of the mesons, the dependencies of the ratio  $R = \Sigma_M^{HT}/\Sigma_M^{LT}$  of the rapidity  $y$  of the meson has a minimum approximately at one point  $y = 1.75$ . After this point, the ratio increases with increasing  $y$ . As seen from calculations with increasing center-of-mass energy from  $\sqrt{s} = 89\text{GeV}$  to  $\sqrt{s} = 209\text{GeV}$ , the distinction between  $R$  decreases for all meson wave functions.

## V. CONCLUDING REMARKS

In this work, we have calculated the higher twist contribution to the large- $p_T$  meson production cross section to show the dependence on the chosen meson wave functions in the process  $\gamma\gamma \rightarrow MX$ . In our calculations, we have used the asymptotic  $\Phi_{asy}$ , Chernyak-Zhitnitsky  $\Phi_{CZ}$ , Braun-Filyanov  $\Phi_{BF}$  wave functions and also, the pion wave function, in which the coefficients  $a_2$  and  $a_4$  have been extracted from the CLEO data on the  $\pi^0\gamma$  transition form factor used. For  $\rho$ -meson we used Ball-Braun wave function. For the high

twist subprocess, we have taken  $\gamma q \rightarrow Mq$ . We have extracted the following two high twist subprocesses  $\gamma q_1 \rightarrow (q_1 \bar{q}_2) q_1$ ,  $\gamma \bar{q}_2 \rightarrow (q_1 \bar{q}_2) \bar{q}_2$  contributing to  $\gamma\gamma \rightarrow MX$  cross sections. As the dominant leading twist subprocess for the meson production, we have taken the photon-photon annihilation  $\gamma\gamma \rightarrow q\bar{q}$ , where the  $M$  meson is indirectly emitted from the quark. The results of our numerical calculations have been plotted in Figs.2-7. As shown in Figs.2,5 the high twist differential cross section monotonically decrease when the transverse momentum of the meson increases. As seen from Figs.2,5 in all wave functions of mesons, the dependencies of the high twist cross sections on the  $p_T$  transverse momentum of the meson demonstrate the same behavior. But, the higher twist corrections are very sensitive to the choice of the meson wave function. It should be noted that the magnitude of the high twist cross section for the pion wave function  $\Phi_{CLEO}(x, Q^2)$  is very close to the asymptotic wave function  $\Phi_{asy}(x)$ .

In Figs.3 and 6, the ratio  $R = \Sigma_M^{HT}/\Sigma_M^{LT}$  has been plotted at  $y = 0$  as a function of the meson transverse momentum,  $p_T$ , for the different meson wave functions. It may be observed that the values of  $R$  for fixed  $y$  and  $\sqrt{s}$  depend on the choice of meson wave function. Within this context, we have also calculated the distinction between  $R(\Phi_{asy}(x))$  and  $R(\Phi_{CLEO}(x, Q^2))$ ,  $R(\Phi_{CZ}(x, Q^2))$ ,  $R(\Phi_{BF}(x, Q^2))$ ,  $R(\Phi_{\rho_L}(x, Q^2))$ ,  $R(\Phi_{\rho_T}(x, Q^2))$ . We have ultimately found that the difference between  $R(\Phi_{asy}(x))$  and  $R(\Phi_{CLEO}(x, Q^2))$  is small, whereas a distinction between  $R(\Phi_{asy}(x))$  with  $R(\Phi_{CZ}(x, Q^2))$ ,  $R(\Phi_{BF}(x, Q^2))$ ,  $R(\Phi_{\rho_L}(x, Q^2))$  and  $R(\Phi_{\rho_T}(x, Q^2))$  is significant. In Figs.4 and 7, the ratio  $R = \Sigma_M^{HT}/\Sigma_M^{LT}$  has been plotted at  $p_T = 7, 17 \text{ GeV}/c$  as a function of the rapidity of the meson for the different meson wave functions. It may be observed that the values of  $R$  for fixed  $p_T$  and  $\sqrt{s}$  depend on the choice of meson wave function. Within this context, we have also calculated the distinction between  $R(\Phi_{asy}(x))$  and  $R(\Phi_{CLEO}(x, Q^2))$ ,  $R(\Phi_{CZ}(x, Q^2))$ ,  $R(\Phi_{BF}(x, Q^2))$ ,  $R(\Phi_{\rho_L}(x, Q^2))$ ,  $R(\Phi_{\rho_T}(x, Q^2))$ . We have ultimately found that the difference between  $R(\Phi_{asy}(x))$  and  $R(\Phi_{CLEO}(x, Q^2))$  is small, whereas a distinction between  $R(\Phi_{asy}(x))$  with  $R(\Phi_{CZ}(x, Q^2))$ ,  $R(\Phi_{BF}(x, Q^2))$ ,  $R(\Phi_{\rho_L}(x, Q^2))$  and  $R(\Phi_{\rho_T}(x, Q^2))$  is significant. Our investigation enables us to conclude that the high twist meson production cross section in the photon-photon collisions depends on the form of the meson model wave functions and may be used for their study. Further investigations are needed in order to clarify the role of high twist effects in QCD.

## Acknowledgments

One of author, A. I. Ahmadov would like to thank Prof. Hans Peter Nilles and also other members of the Physikalisches Institute for appreciates hospitality extended to him in Bonn, where this work has been carried out. The financial support by DAAD is gratefully acknowledged. A. I. Ahmadov is also grateful to NATO Reintegration Grant-980779

---

## VI. REFERENCES

- [1] A.V. Radyushkin, Dubna preprint P2-10717, 1977, hep-ph/0410276.
- [2] V. L. Chernyak and A. R. Zhitnitsky, Nucl. Phys. **B201**, 492 (1982); V. L. Chernyak, A. R. Zhitnitsky and I. R. Zhitnitsky, Nucl. Phys. **B204**, 477 (1982).
- [3] V. L. Chernyak and A. R. Zhitnitsky, Nucl. Phys. **B246**, 52 (1984).
- [4] I. D. King, C. T. Sachrajda, Nucl. Phys. **B279**, 785 (1987).
- [5] V. L. Chernyak, A. R. Zhitnitsky, Phys. Rept. **112**, 173 (1984).
- [6] S. V. Mikhailov and A. V. Radyushkin, JETP Lett. **43**, 712 (1986); Sov. J. Nucl. Phys. **49**, 494 (1989); Phys. Rev. **D45**, 1754 (1992).
- [7] V. M. Braun and I. E. Filyanov, Z. Phys. **C44**, 157 (1989).
- [8] G. R. Farrar, K. Huleihel and H. Zhang, Nucl. Phys. **B349**, 655 (1991).
- [9] V. L. Chernyak, A. A. Ogloblin and I. R. Zhitnitsky, Z. Phys. **C42**, 583 (1989).
- [10] G. R. Farrar, H. Zhang, A. A. Ogloblin and I. R. Zhitnitsky, Nucl. Phys. **B311**, 585 (1988).
- [11] M. Anselmino, P. Kroll and B. Pire, Z. Phys. **C36**, 89 (1987).
- [12] A. V. Radyushkin and R. Ruskov, Phys. Lett. **B374**, 173 (1996); Nucl. Phys. **B481**, 625 (1996).
- [13] S. J. Brodsky and G. L. Lepage, in: Perturbative Quantum Chromodynamics, ed. by A. H. Mueller, p.93, World Scientific (Singapore) 1989.
- [14] S. J. Brodsky, H.-C. Pauli and S. S. Pinsky, Phys. Rept. **301**, 299 (1998).
- [15] The CLEO Collaboration (J. Gronberg *et.al.*), Phys. Rev. **D57**, 33 (1998).
- [16] V. Yu. Petrov, M. V. Polyakov, R. Ruskov, C. Weiss and K. Goeke, Phys. Rev. **D59**, 114018 (1999); hep-ph/9807229.



- [17] J. Qiu and G. Sterman, Nucl. Phys. **B353**, 105, 137 (1991).
- [18] S. J. Brodsky, Int. J. Mod. Phys. **A13**, 2417 (1998).
- [19] J. A. Bagger and J. F. Gunion, Phys. Rev. **D29**, 40 (1984).
- [20] J. A. Bagger and J. F. Gunion, Phys. Rev. **D25**, 2287 (1982).
- [21] J. A. Hassan and J. K. Storrow, Z. Phys. C-Particles and Fields 14, 65 (1982).
- [22] S. J. Brodsky, T. A. DeGrand, J. F. Gunion and J. H. Weis, Phys. Rev. Lett **41**, 672 (1978);  
Phys. Rev. **D19**, 1418 (1979).
- [23] G. P. Lepage and S. J. Brodsky, Phys. Lett. **B87**, 359 (1979); Phys. Rev. Lett. **43**, 545 (1979);  
43, 1625(E) (1979); A. Duncan and A. Mueller, Phys. Rev. **D21**, 1636 (1980).
- [24] G. P. Lepage and S. J. Brodsky, Phys. Rev. **D22**, 2157 (1980).
- [25] A. I. Ahmadov, I. Boztosun, R. Kh. Muradov, A. Soylu and E. A. Dadashov, Int. J. Mod.  
Phys. **E15**, 1209 (2006); hep-ph/0607238.
- [26] E. L. Berger and S. J. Brodsky, Phys. Rev. Lett. **42**, 940 (1979); E. L. Berger, Z. Phys. **C4**,  
289 (1980).
- [27] V. N. Baier and A. G. Grozin, Phys. Lett. **B96**, 181 (1980); S. Gupta, Phys. Rev. **D24**, 1169  
(1981).
- [28] A. Schmedding and O. Yakovlev, Phys. Rev. **D62**, 116002 (2000), hep-ph/9905392.
- [29] P. Ball and V. M. Braun, Phys. Rev. **D54**, 2182 (1996); hep-ph/9602323.
- [30] V. L. Chernyak, Preprint TPI-MINN-91-47-T, December 1991.
- [31] M. A. Shifman, A. I. Vainshtein and V. I. Zakharov, Nucl. Phys. **B147**, 385 (1979).
- [32] F. Cornet, Acta Phys. Polon. **B37**, 663 (2006); hep-ph/0601056.
- [33] B. A. Kniehl, G. Kramer, B. Pötter, Nucl.Phys. **B582**, 514 (2000), hep-ph/0010289.

$p_T, GeV/c$	$\frac{R(\Phi_{CLEO}(x, Q^2))}{R(\Phi_{asy}(x))}$	$\frac{R(\Phi_{CZ}(x, Q^2))}{R(\Phi_{asy}(x))}$	$\frac{R(\Phi_{BF}(x, Q^2))}{R(\Phi_{asy}(x))}$	$\frac{R(\Phi_{BB(L)}(x, Q^2))}{R(\Phi_{asy}(x))}$	$\frac{R(\Phi_{BB(T)}(x, Q^2))}{R(\Phi_{asy}(x))}$
2	0.232	9.054	23.999	3.490	4.048
6	1.492	4.216	5.872	3.950	2.861
14	1.773	1.747	1.216	1.394	1.537
22	0.9499	0.7607	0.68177	0.85668	0.80928
28	0.5568	0.5023	0.7200	0.68469	0.5859
36	0.9874	0.79656	0.6965	0.8766	0.8341

TABLE I: The distinction between  $R(\Phi_{asy}(x))$  with  $R(\Phi_i(x, Q^2))$  (i=CLEO, CZ, BF, BB(L), BB(T)) at c.m. energy  $\sqrt{s} = 89 GeV$ .

$y$	$\frac{R(\Phi_{CLEO}(x, Q^2))}{R(\Phi_{asy}(x))}$	$\frac{R(\Phi_{CZ}(x, Q^2))}{R(\Phi_{asy}(x))}$	$\frac{R(\Phi_{BF}(x, Q^2))}{R(\Phi_{asy}(x))}$	$\frac{R(\Phi_{BB(L)}(x, Q^2))}{R(\Phi_{asy}(x))}$	$\frac{R(\Phi_{BB(T)}(x, Q^2))}{R(\Phi_{asy}(x))}$
-2.25	1.545	1.22	0.745	1.113	1.146
-1.5	0.769	0.594	0.615	0.773	0.714
0.25	1.428	4.183	5.97	2.399	2.893
1.0	0.916	5.169	9.693	2.773	3.276
1.75	0.559	6.936	15.798	3.186	5.549
2.25	0.892	4.922	9.281	2.744	3.529

TABLE II: The distinction between  $R(\Phi_{asy}(x))$  with  $R(\Phi_i(x, Q^2))$  (i=CLEO, CZ, BF, BB(L), BB(T)) at c.m. energy  $\sqrt{s} = 89 GeV$ .

$p_T, GeV/c$	$\frac{R(\Phi_{CLEO}(x, Q^2))}{R(\Phi_{asy}(x))}$	$\frac{R(\Phi_{CZ}(x, Q^2))}{R(\Phi_{asy}(x))}$	$\frac{R(\Phi_{BF}(x, Q^2))}{R(\Phi_{asy}(x))}$	$\frac{R(\Phi_{BB(L)}(x, Q^2))}{R(\Phi_{asy}(x))}$	$\frac{R(\Phi_{BB(T)}(x, Q^2))}{R(\Phi_{asy}(x))}$
20	1.686	2.760	2.865	1.914	2.298
35	1.582	1.507	1.088	1.294	1.413
50	1.014	0.835	0.7266	0.8962	0.8577
65	0.614	0.5534	0.7367	0.70467	0.6017
85	1.011	0.839	0.736	0.0.8977	0.8586
100	1.574	3.368	4.118	2.170	2.637

TABLE III: The distinction between  $R(\Phi_{asy}(x))$  with  $R(\Phi_i(x, Q^2))$  (i=CLEO, CZ, BF, BB(L), BB(T) ) at c.m. energy  $\sqrt{s} = 209 GeV$ .

$y$	$\frac{R(\Phi_{CLEO}(x, Q^2))}{R(\Phi_{asy}(x))}$	$\frac{R(\Phi_{CZ}(x, Q^2))}{R(\Phi_{asy}(x))}$	$\frac{R(\Phi_{BF}(x, Q^2))}{R(\Phi_{asy}(x))}$	$\frac{R(\Phi_{BB(L)}(x, Q^2))}{R(\Phi_{asy}(x))}$	$\frac{R(\Phi_{BB(T)}(x, Q^2))}{R(\Phi_{asy}(x))}$
-2.25	1.571	1.383	0.933	1.212	1.289
-1.5	0.7519	0.616	0.673	0.7689	0.6978
0.25	1.435	3.484	4.626	2.236	2.754
1.0	1.039	4.255	7.252	2.575	3.149
1.75	0.7246	5.887	12.269	2.999	6.338
2.25	1.056	4.003	6.684	2.520	3.295

TABLE IV: The distinction between  $R(\Phi_{asy}(x))$  with  $R(\Phi_i(x, Q^2))$  (i=CLEO, CZ, BF, BB(L), BB(T)) at c.m. energy  $\sqrt{s} = 209 GeV$ .

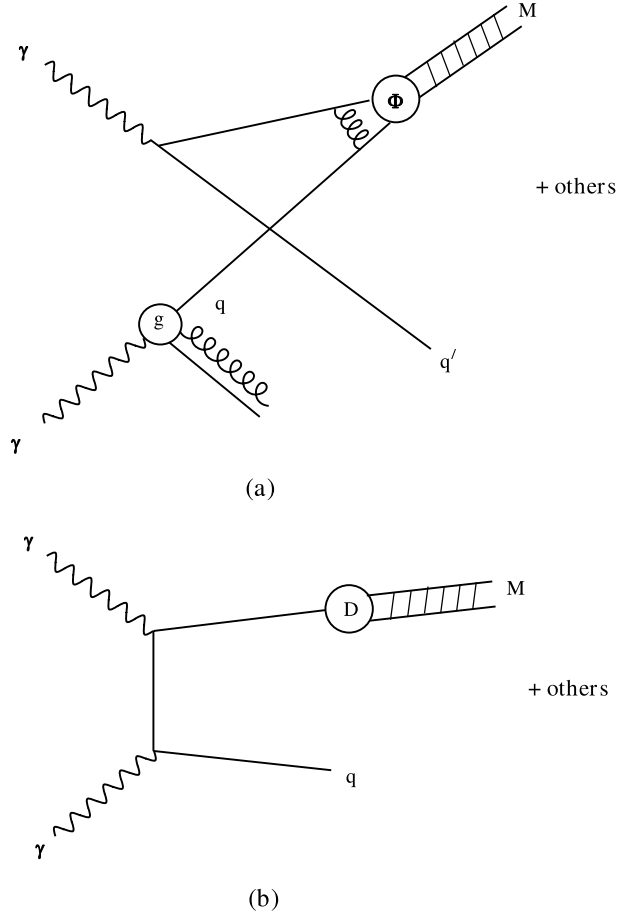


FIG. 1: (a): The higher-twist contribution to  $\gamma\gamma \rightarrow MX$ ; (b): The leading-twist contribution to  $\gamma\gamma \rightarrow MX$

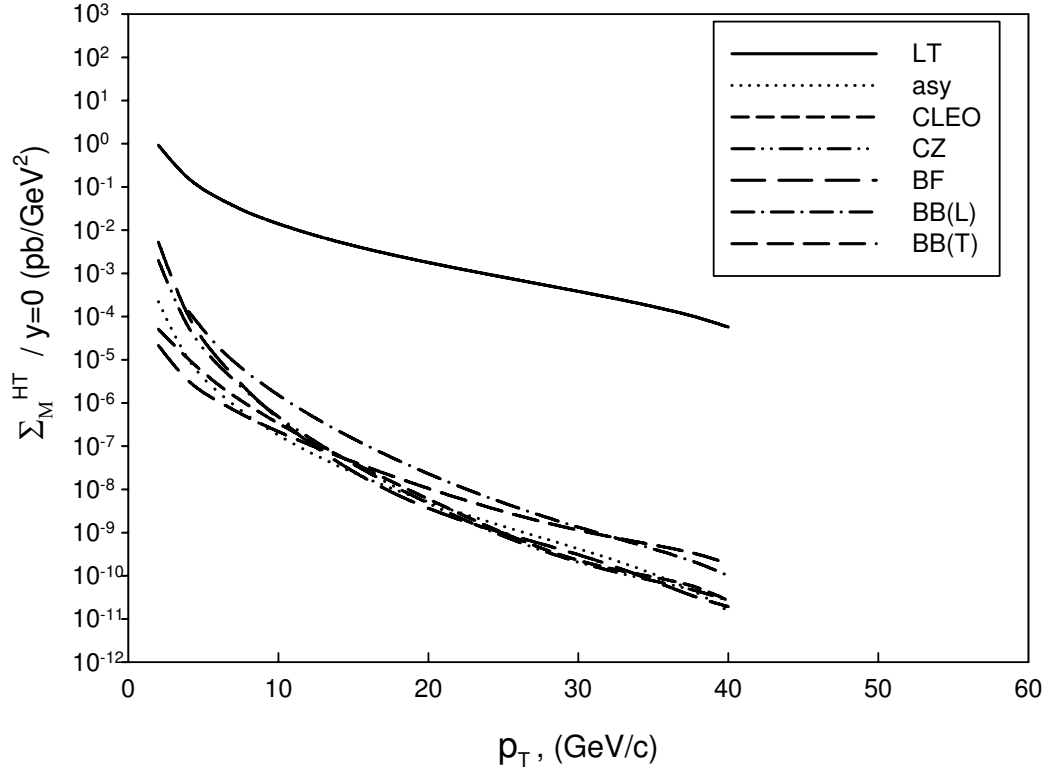


FIG. 2: High twist meson  $M$  production cross sections as a function of the  $p_T$  transverse momentum of the meson at the c.m.energy  $\sqrt{s} = 89 \text{ GeV}$ .

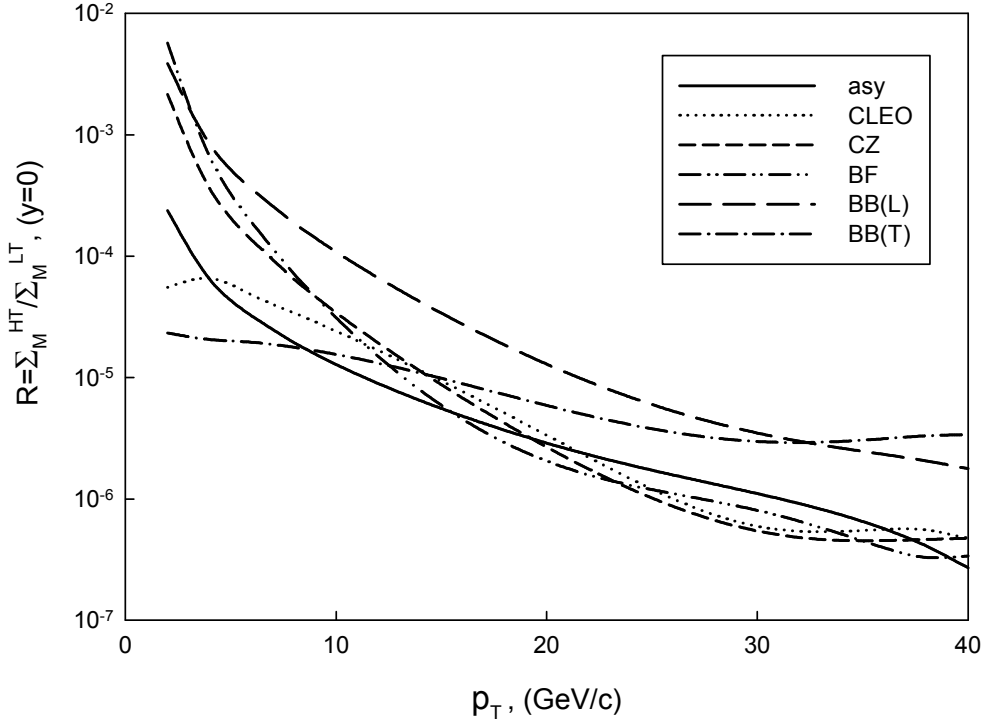


FIG. 3: Ratio  $R = \Sigma_M^{HT} / \Sigma_M^{LT}$ , where the leading and the high twist contributions are calculated for the meson rapidity  $y = 0$  at the c.m. energy  $\sqrt{s} = 89 \text{ GeV}$ , as a function of the meson transverse momentum,  $p_T$ .

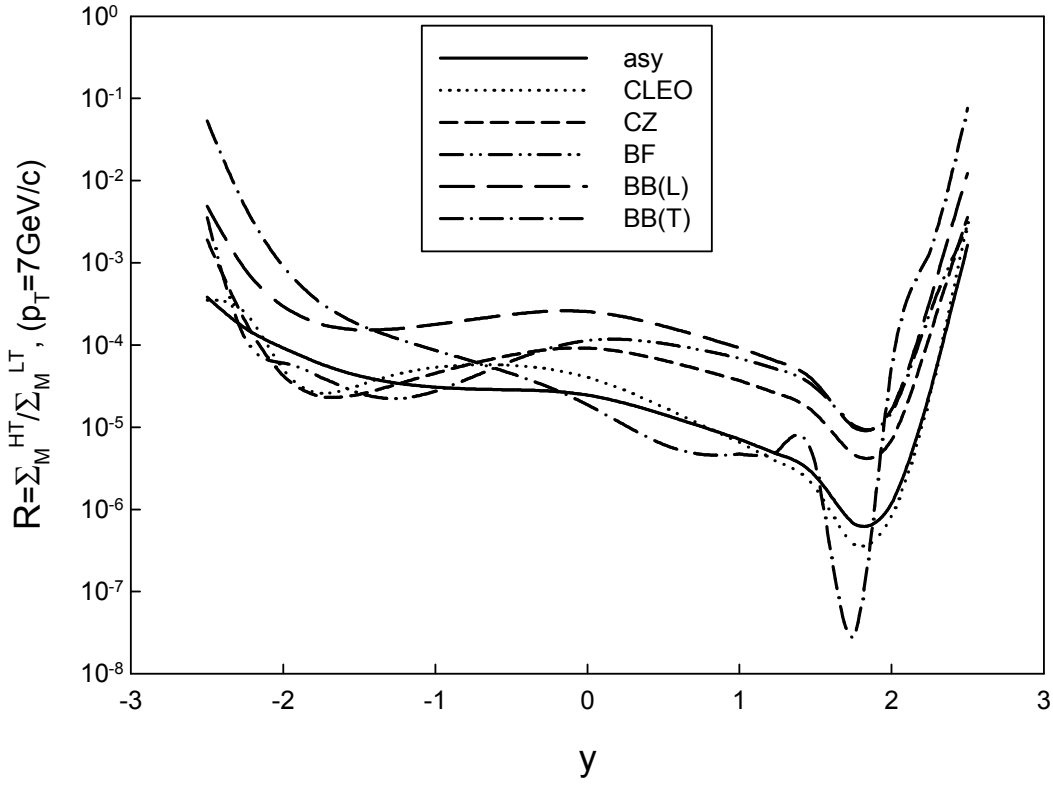


FIG. 4: Ratio  $R = \Sigma_M^{HT} / \Sigma_M^{LT}$ , where the leading and the high twist contributions are calculated for the meson transverse momentum  $p_T = 7 \text{ GeV}/c$  at the c.m. energy  $\sqrt{s} = 89 \text{ GeV}$ , as a function of the  $y$  rapidity of the meson.

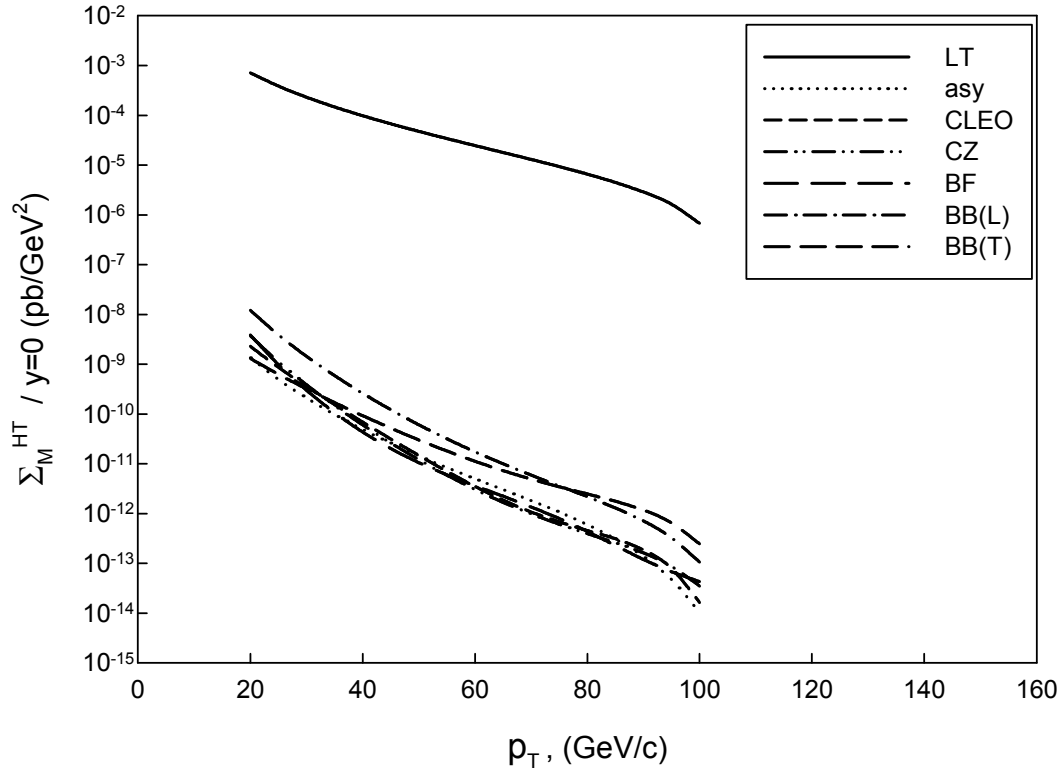


FIG. 5: High twist meson  $M$  production cross sections as a function of the  $p_T$  transverse momentum of the meson at the c.m.energy  $\sqrt{s} = 209 \text{ GeV}$ .

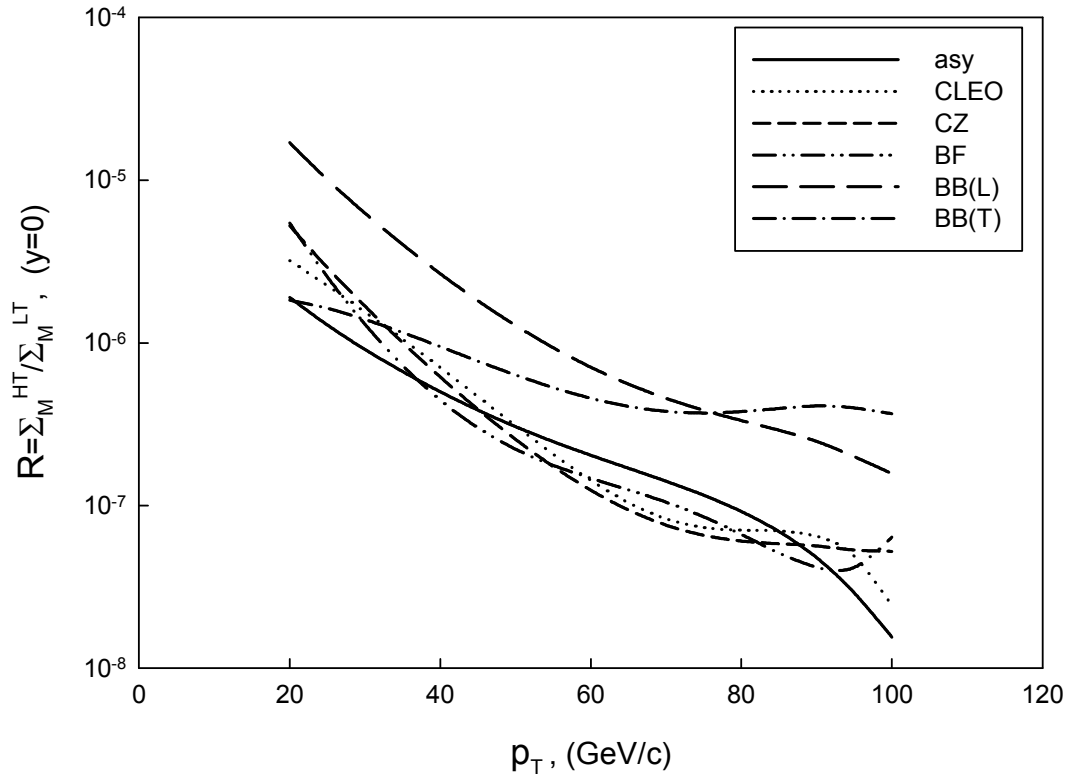


FIG. 6: Ratio  $R = \Sigma_M^{HT} / \Sigma_M^{LT}$ , where the leading and the high twist contributions are calculated for the meson rapidity  $y = 0$  at the c.m. energy  $\sqrt{s} = 209 \text{ GeV}$ , as a function of the meson transverse momentum,  $p_T$ .

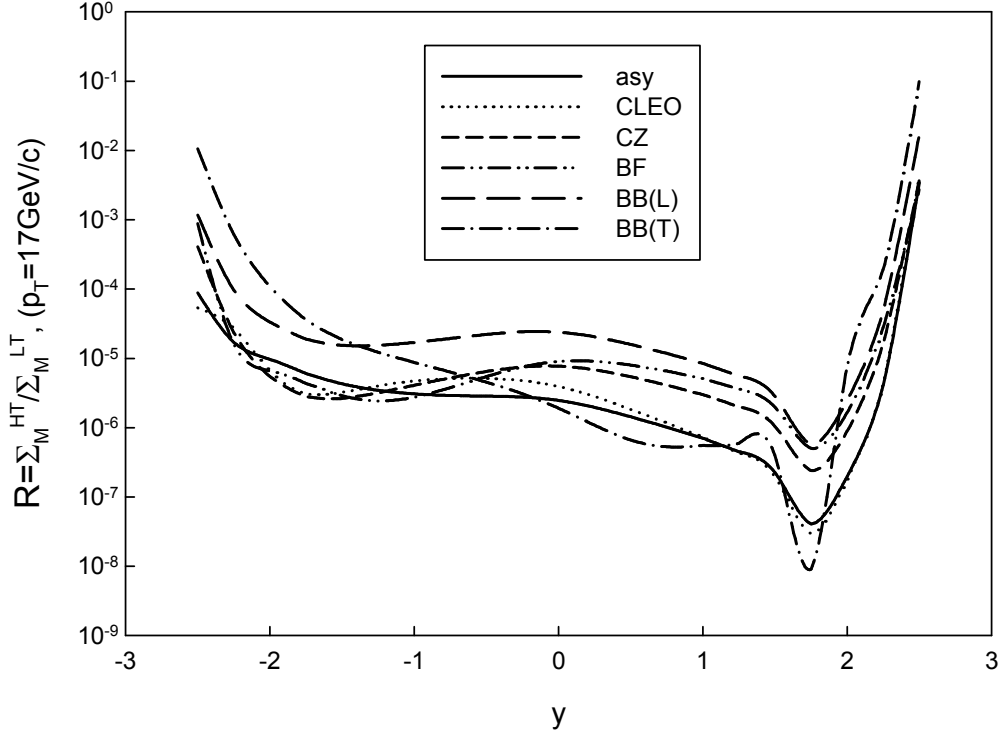


FIG. 7: Ratio  $R = \Sigma_M^{HT} / \Sigma_M^{LT}$ , where the leading and the high twist contributions are calculated for the meson transverse momentum  $p_T = 17 \text{ GeV}/c$  at the c.m. energy  $\sqrt{s} = 209 \text{ GeV}$ , as a function of the  $y$  rapidity of the meson.